Physics – Uspekhi **63** (8) 812 – 817 (2020)

CONFERENCES AND SYMPOSIA

PACS numbers: 52.35.Bj, 52.35.Tc, 52.65.Kj

Heliophysics: from observations to models and applications

V D Kuznetsov, A I Osin

DOI: https://doi.org/10.3367/UFNe.2019.06.038625

Contents

Abstract. Study of the physical phenomena and processes on the Sun and in the heliosphere, a natural plasma laboratory, is based on near-earth and space-based observations and building models which help to obtain a general view of how the Sun was made and how it works, while allowing one to address the practical problems of solar activity influencing space weather and its impact on various areas of human activity. In this paper a brief outline is given of the models of trigger mechanisms driving the most powerful manifestations of solar activity — solar flares and mass ejections, the wave mechanism of solar corona heating. Also, analytical solutions are presented for MHD shock waves in solar wind collisionless plasma with heat fluxes.

Keywords: heliophysics, flares, mass ejections, corona heating, shock waves

1. Introduction

The world of heliophysics, encompassing a great variety of physical objects, processes, and phenomena, is a focus of extensive research efforts. Starting from the interior of the Sun, its atmosphere and the solar wind right up to the boundaries of the Solar system (heliopause), a number of scientific problems arising from the analysis of modern observations remain unresolved. Applied aspects of heliophysics related to the influence of space weather on various areas of human activity on Earth and in outer space tend to attract as much attention from researchers as do its fundamentals [1]. Why are both the amplitude and the length of the 11-year solar cycle, one of the most important manifestations of the Sun's activity — responsible for perturbations of the near-Earth space environment — subjected to such conspicuous changes? The cycle amplitude and length varied from 48 to 190 (the Wolf number) and from 9 to 13.6 years, respectively, over an observation period longer than 300 years. More data on magnetic fields and plasma flows in the convective zone of the Sun and on its surface (especially in polar regions where magnetic field reversal occurs) are needed to answer this and other questions. Also, a more detailed analysis of theoretical solar dynamo models is required. Magnetic fields in circumpolar regions of the Sun will be measured for the first time from out-of-the-ecliptic orbits attainable via gravitational maneuvers near Venus by the Solar Orbiter [2] and Interhelioprobe [3] space missions.

V D Kuznetsov (*), **A I Osin** (**)
Pushkov Institute of Terrestrial Magnetism, Ionosphere and Radio Wave Propagation (IZMIRAN), Russian Academy of Sciences,
Kaluzhskoe shosse 4, 108840 Moscow, Troitsk, Russian Federation
E-mail: (*) kvd@izmiran.ru, (**) osin@izmiran.ru

Received 5 June 2019
Uspekhi Fizicheskikh Nauk **190** (8) 871 – 877 (2020)
Translated by Yu V Morozov; edited by V L Derbov

2. Solar flares and mass ejections

The most powerful manifestations of sporadic activity in the solar atmosphere are associated with flares and mass ejections that cause strong perturbations in Earth's magnetosphere and ionosphere, exert a powerful impact on space equipment performance and terrestrial energy infrastructure [4], create a risk of ionizing radiation exposure for astronauts, and lead to radio and navigation blackouts, breakdown of on-board equipment, and other undesirable consequences. The dependence of satellite and other technologies on space weather patterns driven by the Sun's activity is becoming increasingly more noticeable with their rapid development, which makes necessary careful monitoring and the detailed prediction of solar flares and mass ejections based on the understanding of trigger mechanisms behind these phenomena. The author of Ref. [5] described, using the results from [6], the trigger mechanism of solar flares associated with a rise in the concentration of energetic particles accelerated by the electric field in the current sheet and the trigger mechanism underlying mass ejections [7, 8], in which the twist of the magnetic field of injected magnetic loops plays the key role.

3. Magnetohydrodynamic model for the description of collisionless plasma

Direct measurements of the solar wind plasma in heliospheric regions accessible to spacecraft give evidence of its tempera-

ture anisotropy with respect to the magnetic field direction [9–11]: longitudinal and transverse ion and electron temperatures differ, which implies the use of the temperature-anisotropic collisionless plasma approximation for modeling.

To describe the coronal collisionless plasma and solar wind, the single-fluid eight-moment magnetohydrodynamic (MHD) approximation [12, 13] describing macroscopic characteristics of the plasma is used. The system of MHD equations has the form

$$\frac{\mathrm{d}\rho}{\mathrm{d}t} + \rho\nabla\mathbf{u} = 0\,, \tag{1}$$

$$\rho\frac{\mathrm{d}\mathbf{u}}{\mathrm{d}t} + \nabla\left(p_\perp + \frac{B^2}{8\pi}\right) + (\mathbf{B}\nabla)\left[\left(\frac{p_\parallel - p_\perp}{B^2} - \frac{1}{4\pi}\right)\mathbf{B}\right] = 0\,, \tag{2}$$

$$\frac{\mathrm{d}}{\mathrm{d}t}\left(\frac{p_\parallel B^2}{\rho^3}\right) + \frac{B^2}{\rho^3}\left(\mathbf{B}\nabla\frac{S_\parallel^\parallel}{B} - 2S_\parallel^\perp\mathbf{B}\nabla\frac{1}{B}\right) = 0\,, \tag{3}$$

$$\frac{\mathrm{d}}{\mathrm{d}t}\left(\frac{p_\perp}{\rho B}\right) + \frac{1}{\rho B}\left(\mathbf{B}\nabla\frac{S_\parallel^\perp}{B} + S_\parallel^\perp\mathbf{B}\nabla\frac{1}{B}\right) = 0\,, \tag{4}$$

$$\frac{\mathrm{d}}{\mathrm{d}t}\left(\frac{S_\parallel^\parallel B^3}{\rho^4}\right) + 3\,\frac{p_\parallel B^2}{\rho^4}\mathbf{B}\nabla\frac{p_\parallel}{\rho} = 0\,, \tag{5}$$

$$\frac{\mathrm{d}}{\mathrm{d}t}\left(\frac{S_\parallel^\perp}{\rho^2}\right) + \frac{p_\parallel}{\rho^2 B}\left[\mathbf{B}\nabla\frac{p_\perp}{\rho} + \frac{p_\perp(p_\perp - p_\parallel)}{p_\parallel\rho B}\mathbf{B}\nabla B\right] = 0\,, \tag{6}$$

$$\frac{\mathrm{d}\mathbf{B}}{\mathrm{d}t} = (\mathbf{B}\nabla)\mathbf{u} - \mathbf{B}(\nabla\mathbf{u})\,, \tag{7}$$

$$\nabla\mathbf{B} = 0\,. \tag{8}$$

Here, ρ is the plasma density, $p_\parallel$, $p_\perp$ are the plasma pressures along and across the magnetic field direction, $\mathbf{u}$ is the macroscopic velocity of the plasma, $\mathbf{B}$ is the magnetic field, and $S_\parallel^\parallel, S_\parallel^\perp$ are the heat fluxes along the magnetic field associated with the particles' thermal movements in the longitudinal and transverse directions with respect to the magnetic field, respectively. These equations can be regarded as a generalization of the well-known but very limited Chew–Goldberger–Low (CGL) approximation [14], in the framework of which two adiabatic invariants (Eqns (3) and (4) without heat flux terms) are conserved.

Waves and instabilities within the framework of Eqns (1)–(8) were analyzed in Refs [15–18]. The exact match between fire-hose and mirror instability criteria in terms of this approximation and those given by a kinetic analysis [19] should be noted, in contrast to the CGL approximation, in which the correspondence is valid only for the fire-hose instability. Equations (1)–(8) also describe MHD flow instability.

To distinguish between MHD flux instability and other instabilities, we consider the simplest case of minor perturbations caused by one-dimensional longitudinal movements of the plasma along the magnetic field when the dispersion equation has the form

$$y^4 - 6y^2 - 4\varkappa_\parallel y + 3 = 0\,, \tag{9}$$

where $y = \omega/ka_\parallel$ is the dimensionless phase velocity of waves, and $a_\parallel^2 = p_\parallel/\rho, \varkappa_\parallel = S_\parallel^\parallel/p_\parallel a_\parallel$ is the dimensionless parameter of the longitudinal heat flux component. The $y(\varkappa_\parallel)$ dependence is presented graphically in Fig. 1.

In the case of a zero heat flux ($\varkappa_\parallel = 0$), unlike the CGL approximation, there are two waves, fast and slow, that propagate in either direction at the same speed. In the case of a nonzero thermal flux ($\varkappa_\parallel \neq 0$), the velocities of these waves depend on flux magnitude and direction (see Fig. 1). As the heat flux increases, the velocity of the fast wave increases if it travels in the flux direction but decreases if it propagates against the flux. The reverse situation takes place for the slow wave. At a critical parameter value $\varkappa_\parallel = \pm\varkappa_\parallel^* = \pm[2(\sqrt{2}-1)]^{1/2} \approx \pm 0.91$, the velocities of both waves become equal, which leads to flux instability analogous to flux instability in kinetics [20].

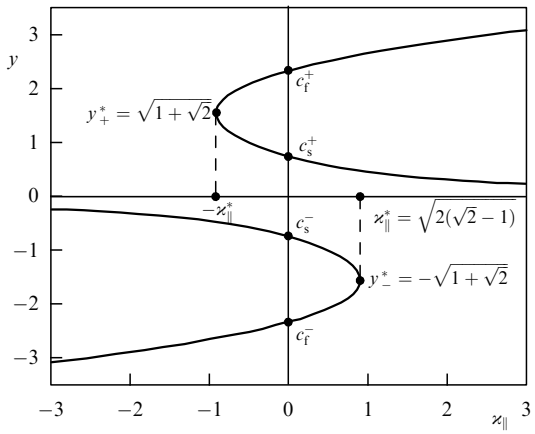

Figure 1. Phase velocities of fast (c_f) and slow (c_s) ion-acoustic waves versus dimensionless heat flux parameter $\varkappa_\parallel$.

In addition to the fast and slow ion-acoustic waves, Eqns (1)–(8) for small perturbations give a thermal wave $\omega/k = a_\parallel$ that can be regarded as an entropy wave modified by heat fluxes [16].

4. Waves and corona heating

Investigations of the solar corona and wind encounter such problems as corona heating up to high temperatures (1–2 mln degrees), shock wave propagation, and turbulence generation.

One of the mechanisms underlying corona heating is associated with dissipation of convection-generated MHD waves whose energy is quite sufficient to maintain high coronal temperature (1–2 mln degrees) [21]. The mechanism of wave propagation up to the corona heights awaits clarification and requires more detailed knowledge of the lower atmosphere structure that can be obtained from high-resolution observations. Such observations are expected to be made during the Parker Solar Probe (NASA), Solar Orbiter (ESA), and Interhelioprobe (Roskosmos) space missions. A sharp rise in temperature is known to occur with increasing altitude in the transition zone between the chromosphere and the corona (Fig. 2), where the heat flux is directed from the corona downward, whereas the wave energy flux along with other energy fluxes maintaining coronal temperature is directed upwards. As a result, waves in the lower corona travel against the heat flux (see above), as shown in Fig. 2. Under certain conditions, this situation may give rise to instability of the waves coming from below accompanied by wave energy dissipation. This instability is due to a heat counterflow that, in turn, somehow depends on wave dissipation and plasma heating. Such a situation can be regarded as a scenario of the self-sustained solar and stellar corona heating mechanism.

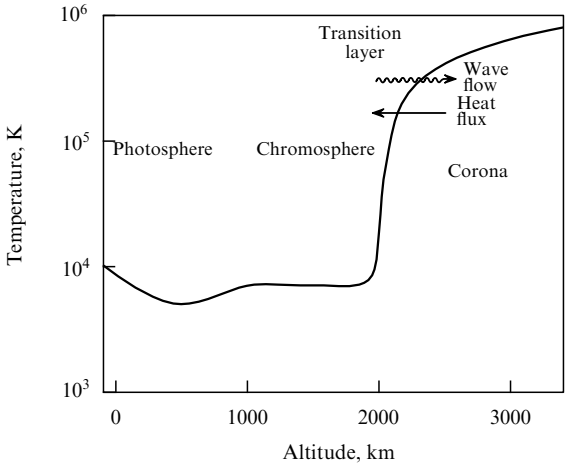

Figure 2. Vertical temperature profile in the Sun's atmosphere and directions of wave and heat flows in the transition layer from the chromosphere to the corona.

Eqn (9) gives the increment of oscillatory flux instability near its threshold value ($|\varkappa_\parallel| \geqslant \varkappa_\parallel^*$):

$$\gamma = ka_\parallel \left[\frac{2}{3}\left(|\varkappa_\parallel| - \varkappa_\parallel^*\right)\right]^{1/2} \left(\frac{1}{2} + \sqrt{\frac{1}{2}}\right)^{1/4}. \tag{10}$$

The large temperature difference between the corona and the transition region allows parameter $\varkappa_\parallel$ to be estimated as $\varkappa_\parallel \leqslant 1$, while the upper bound of the wave vector must be limited by the characteristic scale of the fine structure of the transition region, which is much greater than the characteristic ion gyroradius.

5. Magnetohydrodynamic shock waves and turbulence in collisionless plasma

MHD shock waves in the collisionless plasma of the solar wind were considered in the framework of the CGL approximation and additional assumptions necessary in view of a shortage of equations (conservation laws) due to the presence of two pressures, $p_\parallel$ and $p_\perp$. The relevant references can be found in [22]. For example, the use of an additional equation conserving the magnetic moment of a plasma element (Eqn (4) without heat flux terms) proved unjustified, since measurements in the solar wind did not confirm conservation of the magnetic moment in shock waves [22]. At the same time, local measurements of the ion distribution function in the collisionless solar wind plasma [9–11] gave evidence of heat fluxes that can be taken into consideration with regard to shock waves in the framework of the closed MHD equation system (1)–(8). Estimated values of the heat flux parameter $\varkappa_\parallel$ in the solar wind at different distances from the Sun are presented in [17]. In the vicinity of Earth, $\varkappa_\parallel \approx 0.6-0.9$.

Reference [23] reports the solution for the simplest case of a one-dimensional parallel shock wave propagating along the magnetic field. In this case, the equations for longitudinal and transverse pressure are entirely independent and Eqns (1)–(8) in the divergent form can be written as

$$\frac{\partial \rho}{\partial t} + \frac{\partial(\rho u)}{\partial x} = 0, \tag{11}$$

$$\frac{\partial(\rho u)}{\partial t} + \frac{\partial}{\partial x}(p_\parallel + \rho u^2) = 0, \tag{12}$$

$$\frac{\partial}{\partial t}(p_\parallel + \rho u^2) + \frac{\partial}{\partial x}(S_\parallel^\parallel + 3p_\parallel u + \rho u^3) = 0, \tag{13}$$

$$\frac{\partial p_\perp}{\partial t} + \frac{\partial}{\partial x}(S_\parallel^\perp + p_\perp u) = 0, \tag{14}$$

$$\frac{\partial}{\partial t}\left(S_\parallel^\parallel + 3p_\parallel u + \rho u^3\right) + \frac{\partial}{\partial x}\left(4S_\parallel^\parallel u + 6p_\parallel u^2 + \rho u^4 + \frac{3p_\parallel^2}{\rho}\right) = 0, \tag{15}$$

$$\frac{\partial}{\partial t}(S_\parallel^\perp + p_\perp u) + \frac{\partial}{\partial x}\left(2S_\parallel^\perp u + p_\perp u^2 + \frac{p_\parallel p_\perp}{\rho}\right) = 0. \tag{16}$$

Equations (11)–(16) are related to the laws of conservation of mass, momentum, and energy providing the relevant boundary conditions on a discontinuity. Due to the absence of energy exchange between longitudinal and transverse degrees of freedom in this case, the energy equation splits into two independent equations, (13) and (14). The boundary conditions for heat fluxes $S_\parallel^\parallel$ and $S_\parallel^\perp$ have to be derived from unknown integral laws of conservation, while those obtained from the differential form of the equations can be incorrect [24]. It follows from Eqns (11)–(16) that the terms under $(\partial/\partial x)$ divergence appear in subsequent equations under the partial time derivative. Such symmetric shape of the equations gives reason to suggest that the boundary conditions for thermal fluxes during discontinuity are determined in the case in question by the divergent form of Eqns (15) and (16). As a result, Eqns (11)–(16) yield the following discontinuity boundary conditions:

$$\rho_1 u_1 = \rho_2 u_2, \tag{17}$$

$$p_{\parallel 1} + \rho_1 u_1^2 = p_{\parallel 2} + \rho_2 u_2^2, \tag{18}$$

$$S_{\parallel 1}^\parallel + 3p_{\parallel 1}u_1 + \rho_1 u_1^3 = S_{\parallel 2}^\parallel + 3p_{\parallel 2}u_2 + \rho_2 u_2^3, \tag{19}$$

$$S_{\parallel 1}^\perp + p_{\perp 1}u_1 = S_{\parallel 2}^\perp + p_{\perp 2}u_2, \tag{20}$$

$$4S_{\parallel 1}^\parallel u_1 + 6p_{\parallel 1}u_1^2 + \rho_1 u_1^4 + \frac{3p_{\parallel 1}^2}{\rho_1} = 4S_{\parallel 2}^\parallel u_2 + 6p_{\parallel 2}u_2^2 + \rho_2 u_2^4 + \frac{3p_{\parallel 2}^2}{\rho_2}, \tag{21}$$

$$2S_{\parallel 1}^\perp u_1 + p_{\perp 1}u_1^2 + \frac{p_{\perp 1}p_{\parallel 1}}{\rho_1} = 2S_{\parallel 2}^\perp u_2 + p_{\perp 2}u_2^2 + \frac{p_{\perp 2}p_{\parallel 2}}{\rho_2}, \tag{22}$$

where subscripts 1 and 2 denote the values of physical quantities ahead and behind the shock wave front, respectively. The following dimensionless parameters are used below:

$$Y = \frac{u_2}{u_1} = \frac{\rho_1}{\rho_2}, \quad \alpha = \frac{p_\perp}{p_\parallel},$$

$$a_\parallel^2 = \frac{p_\parallel}{\rho}, \quad a_\perp^2 = \frac{p_\perp}{\rho}, \quad M = \frac{u}{a_\parallel},$$

$$\varkappa_\parallel = \frac{S_\parallel^\parallel}{p_\parallel a_\parallel}, \quad \varkappa_\perp = \frac{S_\parallel^\perp}{p_\perp a_\parallel}.$$

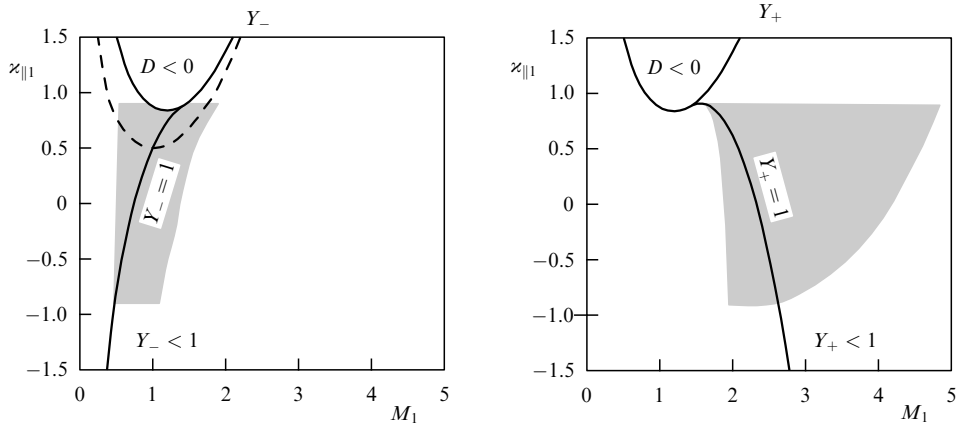

Figure 3. Grey color shows the regions of parameters $\varkappa_{\|1}$ and M_1 for which there is plasma stability ahead of and behind the shock wave front. Curves $Y_\pm = 1$ divide the domain of existence for the solution ($D > 0$) into compression ($Y_\pm < 1$) and rarefaction ($Y_\pm > 1$) subdomains; see the text for details.

Specifically, parameter M_1 is used instead of the Mach number, equaling the ratio of flow velocity ahead of the shock wave front to the phase velocity of the respective small-amplitude wave, depending in the case of interest on parameter $\varkappa_{\|1}$ (see Fig. 1). The following solutions for jumps of physical quantities are obtained from (17)–(22), besides the trivial solution ($Y = 1$) [23]:

$$\frac{\rho_2}{\rho_1} = \frac{1}{Y}\,, \tag{23}$$

$$\frac{u_2}{u_1} = Y\,, \tag{24}$$

$$\frac{p_{\|2}}{p_{\|1}} = 1 + M_1^2 - M_1^2 Y\,, \tag{25}$$

$$\varkappa_{\|1}\frac{S^{\|}_{\|2}}{S^{\|}_{\|1}} = \varkappa_{\|1} + 3M_1 + M_1^3 - 3M_1(1+M_1^2)Y + 2M_1^3 Y^2, \tag{26}$$

$$\frac{p_{\perp 2}}{p_{\perp 1}} = \frac{1}{Y} - 2\frac{\varkappa_{\perp 1} M_1}{Y}\,\frac{1-Y}{2M_1^2 Y - M_1^2 - 1}\,, \tag{27}$$

$$\frac{S^{\perp}_{\|2}}{S^{\perp}_{\|1}} = \frac{M_1^2 - 1}{2M_1^2 Y - M_1^2 - 1} = \frac{M_1^2 - 1}{N(M_1, \varkappa_{\|1})}\,. \tag{28}$$

Here, function $Y = Y(M_1, \varkappa_{\|1})$ has the form

$$\begin{aligned} Y_\pm &= \frac{1}{2}\left(1 + \frac{2}{M_1^2}\right) \pm \sqrt{\frac{1}{12} + \frac{1}{2M_1^4} - \frac{2\varkappa_{\|1}}{3M_1^3}} \\ &= \frac{1}{2}\left(1 + \frac{2}{M_1^2}\right) \pm \sqrt{D}\,, \end{aligned} \tag{29}$$

and the expression with the sign '+' corresponds to either a fast ($M_1 > M_1^* = \sqrt{1+\sqrt{2}}$) or a slow ($M_1 < M_1^*$) wave, and that with the sign '−' to a slow wave (see Fig. 1). In this expression, parameter $\varkappa_{\|1}$ can be both positive and negative, depending on the heat flux direction along or against the direction of wave propagation.

In the plane of parameters $(M_1, \varkappa_{\|1})$ in Fig. 3, the domain of existence for the solution ($D > 0$) is superimposed by the domains in which the plasma ahead of the front ($|\varkappa_{\|1}| < \varkappa_{\|}^*$, the lower and upper boundaries) and behind it ($|\varkappa_{\|2}| < \varkappa_{\|}^*$, the left and right boundaries) is stable with respect to flux instability. The curve $Y_\pm = 1$ divides the set of solutions into compression ($Y_\pm < 1$) and rarefaction ($Y_\pm > 1$) waves. Parameter $\varkappa_{\|2}$ (a dimensionless parameter of the heat flux behind the shock wave front) is given by the formula

$$\begin{aligned} \varkappa_{\|2} &= \frac{S^{\|}_{\|2}}{\rho_2 a^3_{\|2}} \\ &= \frac{\varkappa_{\|1} + 3M_1 + M_1^3 - 3M_1(1+M_1^2)Y + 2M_1^3 Y^2}{\sqrt{Y}(1 + M_1^2 - M_1^2 Y)^{3/2}} \\ &= \varkappa_{\|2}(M_1, \varkappa_{\|1})\,, \end{aligned} \tag{30}$$

defining its dependence on parameters M_1 and $\varkappa_{\|1}$ ahead of the front and, accordingly, the region of these parameters in which turbulence develops behind the shock wave front under the condition that $|\varkappa_{\|2}| > \varkappa_{\|}^*$. Evidently, supercritical values of the heat flux behind the shock wave front can be attained even for a zero flux ahead of the front when the critical numbers for compression waves are $M_{1\mathrm{f}}^* \approx 4.20$ and $M_{1\mathrm{s}}^* \approx 1.37$ for fast and slow shock waves, respectively. This means that in the framework of the MHD approximation a shock wave causes turbulence behind its front at certain values of parameters M_1 and $\varkappa_{\|1}$ (see Fig. 3) due to the aforementioned flux instability. At the kinetic level, the presence of a heat flux behind the shock wave front in this case indicates that the ion distribution function, symmetric ahead of the front, loses symmetry behind it, and the degree of asymmetry is capable of reaching a critical value at which plasma stream instability develops.

Formula (30) can be used to determine the magnitude and direction of the thermal flux behind the shock wave front over the entire plane of parameters $(M_1, \varkappa_{\|1})$ and the respective velocities of small-amplitude waves, which allows them to be used to solve the problem of shock wave evolutionarity by the Landau method [25]. It follows from Eqns (29) and (30) that three curves, $\varkappa_{\|1} = 0$, $\varkappa_{\|2} = 0$, and $Y_\pm = 1$, meet at the same point for both shock waves (fast and slow), thus dividing the entire domain of parameters $(M_1, \varkappa_{\|1})$ restricted by $|\varkappa_{\|1,2}| < \varkappa_{\|}^*$ values into six physically different compression ($Y_\pm < 1$) or rarefication ($Y_\pm > 1$) subdomains with differ-

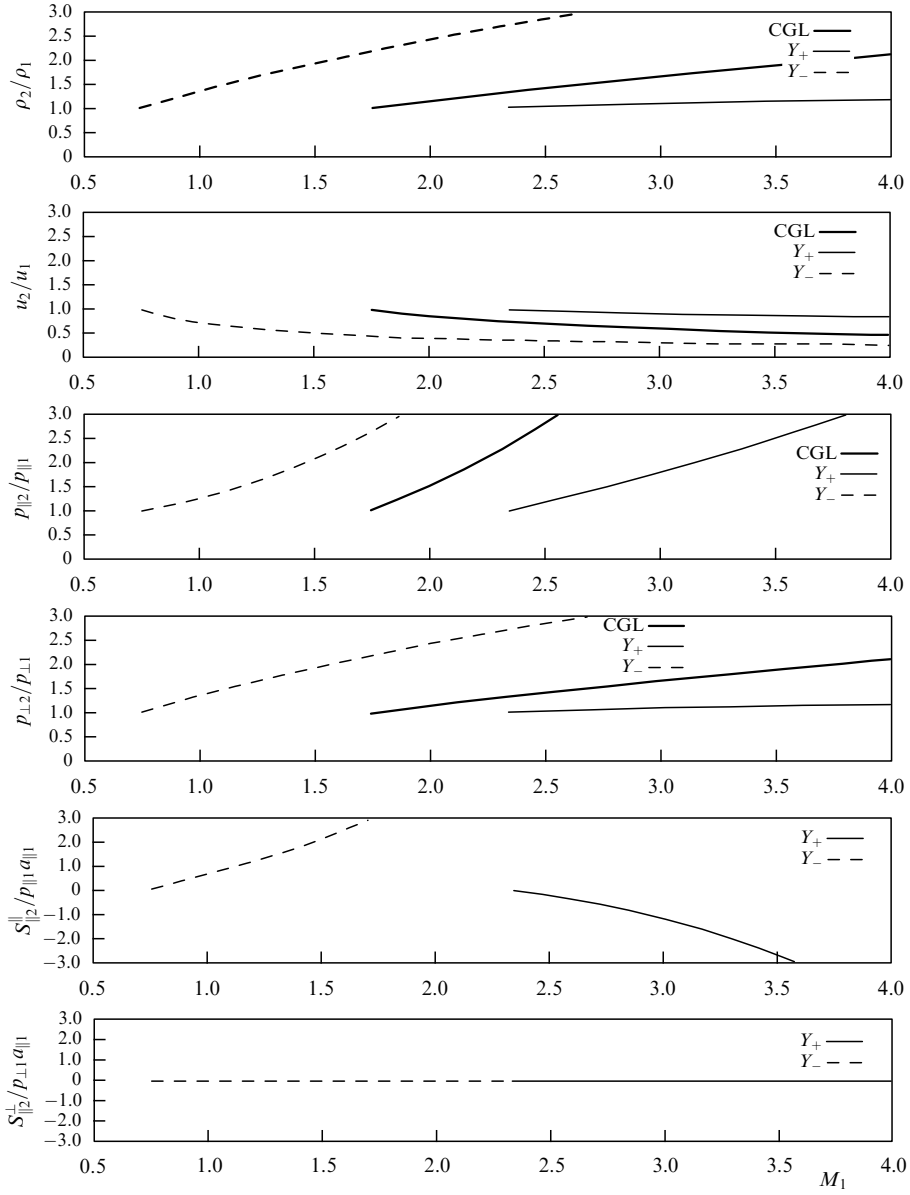

Figure 4. Comparison of the dependences of jumps of physical quantities at slow (dashed lines) and fast (thin solid lines) shock waves on M_1 (for $\varkappa_{\|1} = 0$, $\varkappa_{\perp 1} = 0$) with the solution in the CGL framework (thick solid lines).

ently directed heat fluxes ahead ($S^{\|}_{\|1}$) and behind ($S^{\|}_{\|2}$) the front. A change in the direction and magnitude of the heat flux $S^{\perp}_{\|2}$ behind the shock wave front can be deduced from formula (28).

Figure 4 compares the obtained solutions with one of the solutions in the framework of the CGL approximation [26]. It demonstrates a significant difference in the values of critical number M_1 and jumps of physical quantities.

The solution for a transverse shock wave when the velocity vector is perpendicular to the magnetic field vector can also be obtained from the set of Eqns (1)–(8) [27]. It coincides with the solution in the CGL approximation [14], because the heat fluxes $S^{\|}_{\|}$ and $S^{\perp}_{\|}$ are directed along the magnetic field that is parallel to the shock wave front.

Shock waves in the solar wind plasma are frequently associated with coronal mass ejections and appear in front of the plasma cloud [1]. The study of the character of plasma motion behind the shock wave front is of interest for the verification of the proposed turbulence generation mechanism in the solar wind and the elucidation of the role of this source of turbulence in the general picture of observed solar wind turbulence. The above formulas for jumps of physical quantities measured at shock waves can be used for more detailed diagnostics of the solar wind plasma, including heat fluxes.

A note with regard to the applicability of the MHD approximation being used and limitations on the obtained solutions (23)–(27) is in order. According to [12], the ion distribution function corresponding to the set of Eqns (1)–(8) has the form

$$f = f_0\left\{1 - c_{\|}\left[\frac{\varkappa_{\|}}{2}\left(1 - \frac{2}{3}c_{\|}^2\right) + \alpha\varkappa_{\perp}\left(1 - \frac{1}{2}c_{\perp}^2\right)\right]\right\}, \quad (31)$$

where $c_{\|,\perp} = w_{\|,\perp}/a_{\|,\perp}$ is the dimensionless chaotic constituent of ion velocity and f_0 is the bi-Maxwellian distribution

function

$$f_0 = \frac{n}{(2\pi)^{3/2} a_{\|} a_{\perp}^2} \exp\left(-\frac{c_{\|}^2}{2} - \frac{c_{\perp}^2}{2}\right). \quad (32)$$

The distribution function (31) applicability condition requires that parameters $\varkappa_{\|1}$ and $\varkappa_{\perp 1}$ be small, which implies small deviations of the distribution function from the symmetric bi-Maxwellian distribution function in the kernel region (at low speeds). Plasma flux instability restricts the value of $|\varkappa_{\|}|$ to $\varkappa_{\|}^* \approx 0.91$ (see above). Moreover, the value of $p_{\perp 2}$ can be negative at finite $\varkappa_{\|1}$ and $\varkappa_{\perp 1}$ in the $|\varkappa_{\|1}| < \varkappa_{\|}^*$ region, while the values of $p_{\perp 2}$ and $S_{\|2}^{\perp}$ for a slow shock wave along the $N(M_1, \varkappa_{\|1}) = 0$ $(\varkappa_{\|1} = (M_1^4 + 3)/8M_1)$ curve (the dashed line in Fig. 3) become infinite and the plasma flow velocity u_2 behind the front coincides with the velocity of the thermal wave $a_{\|2}$, i.e., $M_2 = 1$. This curve intersects the curve $Y = 1$ at point $M_1 = 1$, $\varkappa_{\|1} = 1/2$, where three velocities (those of flow u_1, thermal wave $a_{\|1}$, and the slow wave) coincide (see (9)). These features restrict the model applicability region in terms of parameter values $\varkappa_{\|}$ and $\varkappa_{\perp}$. It remains to be elucidated whether these features arise only from the limitations of the MHD model being used (e.g., the requirement that the $\varkappa_{\|}$ and $\varkappa_{\perp}$ parameters be small) or have a deeper physical meaning (nonevolutionarity, wave decay, boundary conditions for heat fluxes, etc.). Nonetheless, the approximation of the function in the form (31) with physically clear characteristics (density, pressure, velocity, heat flux) helps in understanding the role of thermal fluxes that can theoretically exist in a stable collisionless plasma and be detected in the solar wind plasma. For the correct description of distribution function (31) asymmetry, various expressions for its odd part can be considered [28].

6. Conclusion

Theoretical and experimental studies of topical problems of modern heliophysics are aimed at deeper understanding of physical processes underlying the observed phenomena, many of which occur in faraway stars and are important in practical terms for studying space weather, which exerts an increasingly stronger impact on various aspects of human space activity and modern space technologies. The results of research reported in this article represent the authors' contribution to the capacious field of heliophysics, in which observations and physical modeling are paramount for a comprehensive study of the phenomena of interest. The hope for a novel dataset to be delivered by the Parker Solar Probe, Solar Orbiter, and Interhelioprobe space missions is stimulating the development and construction of new models and theoretical concepts in the most interesting and poorly explored areas of heliophysics investigating the Sun and the circumsolar environment as a natural plasma laboratory, a minuscule particle of the multifaceted Universe closest to Earth.

The study was supported by RFBR grant 17-02-01328.

References

1. Bothmer V, Daglis I A *Space Weather*: *Physics and Effects* (Berlin: Springer, 2007)
2. "Solar Orbiter: Exploring the Sun-heliosphere connection", Definition Study Report ESA/SRE(2011)14 (Frascati: European Space Agency, 2011); http://sci.esa.int/solar-orbiter/48985-solarorbiter-definition-study-report-esa-sre-2011-14/
3. Kuznetsov V D, in *Proekt Intergeliozond. Trudy Rabochero Soveshchaniya, Tarusa, 11–13 Maya 2011 g.* (The Interhelioprobe Project. Proc. of the Workshop, Tarusa, May 11–13, 2011) (Ed. V D Kuznetsov) (Moscow: IZMIRAN, 2012) p. 5
4. Kuznetsov V D, Makhutov N A *Herald Russ. Acad. Sci.* **82** 36 (2012); *Vest. Ross. Akad. Nauk* **82** 110 (2012)
5. Kuznetsov V D *Phys. Usp.* **49** 305 (2006); *Usp. Fiz. Nauk* **176** 319 (2006)
6. Gamayunov K V, Oraevsky V N, Kuznetsov V D *Plasma Phys. Control. Fusion* **40** 1285 (1998)
7. Kuznetsov V D, Hood A W *Solar Phys.* **171** 61 (1997)
8. Kuznetsov V D, Hood A W *Adv. Space Res.* **26** 539 (2000)
9. Matteini L et al. *Geophys. Res. Lett.* **34** L20105 (2007)
10. Stansby D et al. *Solar Phys.* **293** 155 (2018)
11. Demars H G, Schunk R W *Planet. Space Sci.* **38** 1091 (1990)
12. Oraevsky V N, Konikov Yu V, Khazanov G V *Protsessy Perenosa v Anizotropnoi Okolozemnoi Plazme* (Transfer Processes in the Anisotropic Circumterrestrial Plasma) (Moscow: Nauka, 1985)
13. Ramos J J *Phys. Plasmas* **10** 3601 (2003)
14. Chew G F, Goldberger M I, Low F E *Proc. R. Soc. Lond. A* **236** 112 (1956)
15. Namikawa T, Hamabata H *Phys. Lett. A* **81** 339 (1981)
16. Namikawa T, Hamabata H *J. Plasma Phys.* **26** 95 (1981)
17. Zakharov V Yu, in *Voprosy Magnitnoi Gidrodinamiki Plazmy bez Stolknovenii v Sil'nom Magnitnom Pole* (Eds G A Lyubimov, I S Shikin) (Moscow: Izd. MGU, 1988) p. 48
18. Kuznetsov V D, Dzhalilov N S *Plasma Phys. Rep.* **35** 962 (2009); *Fiz. Plazmy* **35** 1041 (2009)
19. Vedenov A A, Sagdeev R Z, in *Plasma Physics and the Problem of Controlled Thermonuclear Reactions* Vol. 3 (Ed. M A Leontovich) (New York: Pergamon Press, 1961) p. 332; Translated from Russian: in *Fizika Plazmy and Problema Upravlyaemykh Termoyadernykh Reaktsii* Vol. 3 (Ed. M A Leontovich) (Moscow: Izd. AN SSSR, 1958) p. 278
20. Dzhalilov N S, Kuznetsov V D *Plasma Phys. Rep.* **39** 1026 (2013); *Fiz. Plazmy* **39** 1122 (2013)
21. Aschwanden M J *Physics of the Solar Corona*: *an Introduction with Problems and Solutions* (Berlin: Springer, 2006)
22. Baranov V B, Krasnobaev K V *Gidrodinamicheskaya Teoriya Kosmicheskoi Plazmy* (The Hydrodynamic Theory of Cosmic Plasma) (Moscow: Nauka, 1977)
23. Kuznetsov V D, Osin A I *Phys. Lett. A* **382** 2052 (2018)
24. Akhiezer A I et al. *Plasma Electrodynamics* (Oxford: Pergamon Press, 1975); Translated from Russian: *Elektrodinamika Plazmy* (Moscow: Nauka, 1974)
25. Landau L D, Lifshitz E M *Fluid Mechanics* (Oxford: Pergamon Press, 1987); Translated from Russian: *Gidrodinamika* (Moscow: Nauka, 1986)
26. Morioka S, Spreiter J R *J. Plasma Phys.* **2** 449 (1968)
27. Kuznetsov V D, Osin A I, in *Proc. of the Intern. Conf. in Honor of Professor Konstantin I. Gringauz 100th Birthday*: *Gringauz 100*: *Plasmas in the Solar System, June 13–15, 2018, Moscow, Russia* (Moscow: Space Research Institute of RAS, 2018) p. 153
28. Whang Y C *J. Geophys. Res.* **76** 7503 (1971)